Ab initio calculations of elastic constants and thermodynamic properties of bcc, fcc, and hcp Al crystals under pressure

2002 J. Phys.: Condens. Matter 14 6989

(http://iopscience.iop.org/0953-8984/14/29/301)

INSTITUTE OF PHYSICS PUBLISHING JOURNAL OF PHYSICS: CONDENSED MATTER

J. Phys.: Condens. Matter **14** (2002) 6989–7005 PII: S0953-8984(02)36802-4

Ab initio calculations of elastic constants and thermodynamic properties of bcc, fcc, and hcp Al crystals under pressure

G V Sin'ko and N A Smirnov

Federal Nuclear Centre, Institute of Technical Physics, Snezhinsk 456770, Russia

E-mail: g.v.sinko@vniitf.ru

Received 9 May 2002
Published 11 July 2002
Online at stacks.iop.org/JPhysCM/14/6989

Abstract

We have performed *ab initio* electronic structure and total-energy calculations for bcc, fcc, and hcp Al structures to study the equations of state, volume dependences of elastic constants, and relative stability diagram for these structures. A technique for elastic constant calculation in the case of initial isotropic pressure is presented. In this study we used the accurate full-potential linear muffin-tin orbital method to describe electrons of the crystal and the Debye treatment of the vibrating lattice. The volume dependence of the Debye temperature is derived from the volume dependence of the elastic constants. Our calculations show that at pressures of 1–2 Mbar and temperatures of about 1000 K and higher, the aluminium structure must have a lower symmetry than the structures considered.

1. Introduction

Interest in *ab initio* (without empirical parameters) calculations of the equation of state (EOS) and relative stability of crystal structures has been high for many years. As a rule, calculations have been done for $T = 0$, where there is no thermal excitation of nuclei. In particular, the relative stability of the fcc, bcc, and hcp structures of Al was studied in [1–7] for static lattices with the use of different electron structure calculation methods and different forms of the exchange–correlation functional.

Also, attempts were made to allow for the contribution of the thermal excitation of nuclei to thermodynamic functions without using empirical parameters. There are two directions followed in those attempts. The first uses the Debye model; the second is based on the approximate construction of the phonon dispersion relations. These approaches were widely used previously for construction of the semi-empirical EOS. In particular, a well-known form of the EOS, named the Mie–Grüneisen form [8], was based on the Debye model. The new

feature, which allows us to describe the results as *ab initio*, is the use of values obtained in *ab initio* calculations instead of empirical parameters.

Moruzzi *et al* [9] described thermal excitation of nuclei within the scope of the Debye model, which incorporated a volume dependence of the Debye temperature. They expressed this dependence in terms of a volume dependence of the bulk modulus, which had been obtained from *ab initio* calculations. An attempt to investigate systematically the influence of temperature on thermodynamic functions of different Al crystal structures in terms of *ab initio* calculations was made in our previous paper [10]. Similarly to Moruzzi *et al* [9], we used the Debye model for the description of thermal excitation of the nuclei, but unlike them, we determined the relationships of the shear modulus (S) and longitudinal modulus (L) with the bulk modulus (B) individually for each structure by averaging over periodic system elements having similar crystal structure. Unfortunately, this approach allowed us to reach only qualitative conclusions about the influence of temperature on the relative stability of fcc, bcc, and hcp structures of Al.

Christensen *et al* [11] considered bcc and fcc structures of Cs within the scope of the quasi-harmonic approximation, obtained the phonon dispersion relation in terms of elastic constants, and used *ab initio* elastic constants as functions of volume to calculate the basic thermodynamical functions of bcc and fcc structures and the fcc–bcc coexistence pressure versus temperature for Cs. Katsnelson *et al* [12] used a pseudopotential model for calculation of the phonon contribution to thermodynamical functions. Debernardi *et al* [13] also used the pseudopotential model for calculation of the phonon dispersion relation. To obtain the phonon frequencies as functions of volume, they used Taylor expansion and perturbation theory. As a result, temperature dependences of the linear thermal expansion coefficient and of the specific heat were obtained for aluminium and tungsten.

Mohn *et al* [14] presented a mean-field model for temperature-induced martensitic phase transitions. The classical mean-field potential approach was used successfully in a paper by Wang and Li [15] to evaluate the vibrational contribution of the Al fcc lattice ions to the total free energy. Unfortunately, the mean-field potential used in [15] depends weakly on the crystal structure and, therefore, cannot be used for evaluation of the vibrational free energy of the other Al structures.

Molecular dynamics simulations were also used for the description of the thermal excitation of nuclei without using empirical parameters. Strachan *et al* [16] used this method to predict the EOS and the phase coexistence curves of the B1–B2 and B1–liquid phases of MgO.

Cohen and Gülseren [17] obtained the contribution of the thermal excitation of nuclei by computing the partition function using the particle-in-a-cell model. This incomplete list of works corroborates our assertion of a high level of interest in *ab initio* calculations of the influence of temperature on thermodynamic functions.

In this paper we present revised and more complete [7] theoretical data on the EOS and volume dependence of the elastic constants for Al in bcc, fcc, and hcp structures at $T = 0$. These data were obtained by means of the high-precision full-potential linear muffin-tin orbital (FPLMTO) method [18]. Also, the influence of temperature on the thermodynamic functions of the fcc, bcc, and hcp structures of Al is studied. For this we used a variant of the Debye model [19] where the volume dependence of the Debye temperature was found by using the volume dependence of the elastic constants at $T = 0$. Thermal excitation of electrons was taken into account, too. An attempt was made to construct the P–T diagram of the relative stability of the fcc, bcc, and hcp crystal structures of Al, and existence of an unknown structure was predicted. This structure exists at elevated temperatures and pressures of 1–2 Mbar. Preliminary results of this work were published in [20–22].

The rest of this paper is organized as follows. The technique used for the elastic constant calculation in the case of initial isotropic pressure is given in section 2. Computational details of the *ab initio* electronic structure calculations and the method used for the thermodynamic function calculations are given in section 3. In section 4 we present the calculations of the EOS, elastic constants, Debye temperature, and Grüneisen parameter for various Al structures at various specific volumes. In section 4 we report on the results of the construction of the relative stability diagram for fcc, bcc, and hcp Al structures, too. Finally, a short summary is given in section 5.

2. Elastic constants under pressure

2.1. The method of the elastic constant calculation

At present, *ab initio* calculations of elastic constants of crystals under ambient pressure are not a problem (see, e.g., [23–32]). However, the question of how to calculate elastic constants at arbitrary isotropic pressure requires special consideration. We managed to find only a few papers [33–36] concerning this problem.

Let us consider a crystal compressed by the isotropic pressure P to the density ρ_1. Small (but not infinitesimal) homogeneous deformation of this crystal takes every Bravais lattice point $\vec{R}$ of the undistorted lattice to a new position $\vec{R}'$ in the strained lattice:

$$R'_i = \sum_j (\delta_{ij} + \varepsilon_{ij}) R_j. \tag{1}$$

For a homogeneous strain the parameters ε_{ij} are simply constants, independent of $\vec{R}$, with $\varepsilon_{ij} = \varepsilon_{ji}$, where the subscripts i, j indicate Cartesian components and each ranges over three values; δ_{ij} is the Kronecker delta. Expanding the internal energy per unit mass of the crystal with respect to the Lagrangian strain tensor:

$$\eta_{ij} = \varepsilon_{ij} + \tfrac{1}{2} \sum_k \varepsilon_{ik}\varepsilon_{kj} \tag{2}$$

gives [37]

$$E(\rho_1, \{\eta_{mn}\}) = E(\rho_1) + \frac{1}{\rho_1}\left(\sum_{ij} T_{ij}\eta_{ij} + \frac{1}{2} \sum_{ijkl} C_{ijkl}\eta_{ij}\eta_{kl} + \cdots \right). \tag{3}$$

Here T_{ij} stands for components of the stress tensor before deformation:

$$T_{ij} = \rho_1 \left. \frac{\partial E(\rho_1, \{\eta_{mn}\})}{\partial \eta_{ij}} \right|_{\{\eta_{mn}=0\}}. \tag{4}$$

For isotropic initial pressure, we have

$$T_{ij} = -P\delta_{ij}. \tag{5}$$

C_{ijkl} are elastic constants of the crystal at an arbitrary isotropic pressure P:

$$C_{ijkl} = \rho_1 \left. \frac{\partial^2 E(\rho_1, \{\eta_{mn}\})}{\partial \eta_{ij}\, \partial \eta_{kl}} \right|_{\{\eta_{mn}=0\}}. \tag{6}$$

It should be pointed out that equation (3) represents the energy of the strained crystal in the case of full relaxation of atom positions within the distorted Bravais lattice.

To calculate *ab initio* elastic constants, the deformation parameters are usually specified in the form $\varepsilon_{ij} = f_{ij}(\gamma)$, where γ is an infinitesimal parameter and $f_{ij}(0) = 0$. If equations (2), (5) are used and ε_{ij} is represented in the form

$$\varepsilon_{ij} = s_{ij}\gamma + e_{ij}\gamma^2 + \cdots, \tag{7}$$

then equation (3) can be written as follows:

$$E(\rho_1, \{\eta_{mn}\}) = E(\rho_1) + A\gamma + \frac{D}{2}\gamma^2 + \cdots, \tag{8}$$

where

$$A = -\frac{P}{\rho_1}\sum_i s_{ii}, \tag{9}$$

$$D = \frac{1}{\rho_1}\sum_{ijkl} C_{ijkl}s_{ij}s_{kl} - \frac{2P}{\rho_1}\sum_{ik}\left(e_{ik}\delta_{ik} + \frac{s_{ik}^2}{2}\right). \tag{10}$$

By present-day *ab initio* methods, one can calculate the energy of a strained crystal as a function of γ for any initial isotropic pressure P and any deformation parameters ε_{ij} of the form (7), and obtain the linear equation for elastic constants C_{ijkl}:

$$\sum_{ijkl} C_{ijkl}s_{ij}s_{kl} = 2P\sum_{ik}\left(e_{ik}\delta_{ik} + \frac{s_{ik}^2}{2}\right) + \rho_1\frac{\partial^2 E(\rho_1, \gamma)}{\partial\gamma^2}\bigg|_{\gamma=0}. \tag{11}$$

We ought to note that equation (11) is equally valid for strains with and without volume conservation. Obviously, for ambient conditions equation (11) is in agreement with ones which were used before [23–32]. In order to calculate all M independent elastic constants of a crystal, we need to apply M independent strains to the unit cell and to obtain a system of M linear equations, each being like equation (11).

Using the symmetry properties of matrices $\hat{\varepsilon}$ and $\hat{C}$, the standard notation $xx \equiv 1$, $yy \equiv 2$, $zz \equiv 3$, $yx \equiv 4$, $zx \equiv 5$, $yz \equiv 6$, and introducing a value

$$\xi_\alpha = \begin{cases} 1, & \text{if } \alpha = 1, 2, 3 \\ 2, & \text{if } \alpha = 4, 5, 6, \end{cases} \tag{12}$$

we can rewrite equation (11) as

$$\sum_{\alpha\beta}\xi_\alpha\xi_\beta C_{\alpha\beta}s_\alpha s_\beta = 2P\sum_\alpha(2 - \xi_\alpha)e_\alpha + P\sum_\alpha \xi_\alpha s_\alpha^2 + \rho_1\frac{\partial^2 E(\rho_1, \gamma)}{\partial\gamma^2}\bigg|_{\gamma=0}. \tag{13}$$

According to equation (13), pressure has an influence on the values of the elastic constants even when isochoric strains are used. The authors of [36] did not take this fact into account; therefore their high-pressure elastic constants for tantalum need refinement.

2.2. Bulk modulus and elastic constants

Let us consider the strain representing the crystal response to hydrostatic pressure (all-sides compression). This strain allows determination not only of the value of some linear combination of the elastic constants but also of the link between the elastic constants and the bulk modulus. As an example, below we will consider this link for a tetragonal crystal which has been compressed by isotropic pressure P to a density of $\rho_1 = 1/V_1$.

For real tetragonal crystals the parameter c/a is a function of specific volume V:

$$\frac{c}{a} \equiv \varphi(V) = \varphi(V_1)\left[1 + \frac{\mu}{V_1}(V - V_1) + \cdots\right], \tag{14}$$

where

$$\mu = \frac{V_1}{\varphi(V_1)}\frac{\mathrm{d}\varphi(V)}{\mathrm{d}V}\bigg|_{V=V_1}. \tag{15}$$

The all-sides compression corresponds to a strain

$$\varepsilon_{ij} = t_i(\gamma)\delta_{ij}. \tag{16}$$

Here $t_1 = t_2 = \gamma$, $t_3 = \beta(\gamma)$, and the function $\beta(\gamma)$ is specified by the volume dependence of the parameter c/a:

$$\frac{c}{a} = \frac{1+\beta(\gamma)}{1+\gamma}\varphi(V_1). \tag{17}$$

Comparing equations (14) and (17) and taking into account that the specific volume for the strain (16) correlates with γ as

$$V = V_1(1+\gamma)^2(1+\beta(\gamma)), \tag{18}$$

we derive

$$\beta(\gamma) = \frac{(1-\mu)(1+\gamma)}{1-\mu(1+\gamma)^3} - 1. \tag{19}$$

Since the crystal energy for the strain (16) is a function of specific volume only, using equations (18), (19) and the definitions

$$P = -\frac{\mathrm{d}E}{\mathrm{d}V}, \qquad B = V\frac{\mathrm{d}^2E}{\mathrm{d}V^2}, \tag{20}$$

we can obtain the following result:

$$\rho_1 \frac{\mathrm{d}^2E}{\mathrm{d}\gamma^2}\bigg|_{\gamma=0} = \frac{B}{V_1^2}\left(\frac{\mathrm{d}V}{\mathrm{d}\gamma}\right)^2\bigg|_{\gamma=0} - \frac{P}{V_1}\frac{\mathrm{d}^2V}{\mathrm{d}\gamma^2}\bigg|_{\gamma=0} = \frac{9B}{(1-\mu)^2} - 6\frac{1+2\mu}{(1-\mu)^2}P. \tag{21}$$

For tetragonal crystals there are six independent elastic constants, usually referred to as $C_{11}, C_{12}, C_{13}, C_{33}, C_{44}, C_{66}$, with the rest defined by symmetry and the equalities

$$C_{22} = C_{11}, \qquad C_{23} = C_{13}, \qquad C_{55} = C_{44}, \tag{22}$$

or equal to zero.

Equations (13), (16), (18)–(22) lead to the following relationship between the elastic constants and bulk modulus for tetragonal crystals:

$$2C_{11} + 2C_{12} + 4\frac{1+2\mu}{1-\mu}C_{13} + \left(\frac{1+2\mu}{1-\mu}\right)^2 C_{33} = \frac{9B}{(1-\mu)^2} - 3\frac{1-4\mu^2}{(1-\mu)^2}P. \tag{23}$$

In the case of $P = 0$, equation (23) gives

$$2C_{11} + 2C_{12} + 4\frac{1+2\mu}{1-\mu}C_{13} + \left(\frac{1+2\mu}{1-\mu}\right)^2 C_{33} = \frac{9B}{(1-\mu)^2}. \tag{24}$$

Moreover, if the c/a ratio does not change, equation (24) coincides with the familiar relationship

$$B = \tfrac{1}{9}(2C_{11} + 2C_{12} + 4C_{13} + C_{33}). \tag{25}$$

It is easy to verify that equation (23) is true not only for tetragonal crystals, but also for hexagonal ones.

For cubic crystals, the relationship between elastic constants and the bulk modulus is

$$C_{11} + 2C_{12} = 3B - P. \tag{26}$$

This relationship generalizes the one known (see [38]) for the case of $P > 0$ and can be derived from equation (23) if the identities valid for cubic crystals $C_{33} = C_{11}$, $C_{13} = C_{12}$ are used and the c/a ratio is assumed to be constant. The relationship (26) was used in [39].

2.3. Mechanical stability in crystals under isotropic pressure

Using equations (8)–(10) we can state the conditions for mechanical stability of a crystal against any homogeneous elastic deformation (1). To do this, let us represent equation (8) as follows:

$$\Delta E = E(\rho_1, \gamma) - E(\rho_1, 0) = -P\,\Delta V + \Delta E_{in}, \tag{27}$$

where ΔV is the variation of the volume with deformation:

$$\begin{aligned}\Delta V &= V_1[\det(\hat{I} + \hat{\varepsilon}) - 1] \\ &= V_1\gamma\left(\sum_i s_{ii}\right) + \frac{V_1\gamma^2}{2}\left[2\left(\sum_i e_{ii}\right) + \left(\sum_i s_{ii}\right)^2 - \sum_{ij} s_{ij}^2\right] + \cdots, \end{aligned}\tag{28}$$

$$\begin{aligned}\Delta E_{in} &= V_1\frac{\gamma^2}{2}\left[P\left(\sum_i s_{ii}\right)^2 - 2P\sum_{ij} s_{ij}^2 + \sum_{ijkl} C_{ijkl}s_{ij}s_{kl}\right] + \cdots \\ &= V_1\frac{\gamma^2}{2}\sum_{\alpha\beta}\{\xi_\alpha\xi_\beta C_{\alpha\beta} + P[(2-\xi_\alpha)(2-\xi_\beta) - 2\xi_\alpha\delta_{\alpha\beta}]\}s_\alpha s_\beta + \cdots \\ &= V_1\frac{\gamma^2}{2}\sum_{\alpha\beta} G_{\alpha\beta}s_\alpha s_\beta + \cdots. \end{aligned}\tag{29}$$

The requirement of mechanical stability of the crystal leads to the inequality $\Delta E_{in} > 0$. This inequality is satisfied only if a symmetric matrix

$$\hat{G} = \begin{bmatrix} \tilde{C}_{11} & \tilde{C}_{12} & \tilde{C}_{13} & 2C_{14} & 2C_{15} & 2C_{16} \\ \tilde{C}_{21} & \tilde{C}_{22} & \tilde{C}_{23} & 2C_{24} & 2C_{25} & 2C_{26} \\ \tilde{C}_{31} & \tilde{C}_{32} & \tilde{C}_{33} & 2C_{34} & 2C_{35} & 2C_{36} \\ 2C_{41} & 2C_{42} & 2C_{43} & 4\tilde{C}_{44} & 4C_{45} & 4C_{46} \\ 2C_{51} & 2C_{52} & 2C_{53} & 4C_{54} & 4\tilde{C}_{55} & 4C_{56} \\ 2C_{61} & 2C_{62} & 2C_{63} & 4C_{64} & 4C_{65} & 4\tilde{C}_{66} \end{bmatrix} \tag{30}$$

has a positive determinant. Here,

$$\begin{aligned} &\tilde{C}_{\alpha\alpha} = C_{\alpha\alpha} - P, \qquad \alpha = 1, 2, \ldots, 6 \\ &\tilde{C}_{12} = C_{12} + P, \qquad \tilde{C}_{13} = C_{13} + P, \qquad \tilde{C}_{23} = C_{23} + P. \end{aligned}\tag{31}$$

This result agrees with one published several years ago [40].

For cubic crystals, a positive determinant for matrix (30) and therefore mechanical stability of the crystals occurs under the following conditions:

$$\tilde{C}_{44} > 0, \qquad \tilde{C}_{11} > |\tilde{C}_{12}|, \qquad \tilde{C}_{11} + 2\tilde{C}_{12} > 0. \tag{32}$$

For hexagonal crystals, these conditions are more complex:

$$\tilde{C}_{44} > 0, \qquad \tilde{C}_{11} > |\tilde{C}_{12}|, \qquad \tilde{C}_{33}(\tilde{C}_{11} + \tilde{C}_{12}) > 2\tilde{C}_{13}^2. \tag{33}$$

For ambient conditions, equations (32), (33) are in agreement with familiar expressions.

3. The method of thermodynamic function calculation

3.1. Static zero-temperature energy and pressure calculation

Our calculations of the static zero-temperature energy for the fcc, bcc, and hcp Al structures are based on first-principles density-functional theory within the generalized gradient approximation [41, 42]. The calculations were all-electron, non-relativistic and employed no

shape approximation for the charge density or potential. We used the highly accurate FPLMTO technique [18]. The calculations were done for one, fully hybridized energy panel, in which 2s, 2p, 3s, 3p electrons of the Al atom were included. The basis set was comprised of augmented linear muffin-tin orbitals with s, p, d momenta. The angular momentum representation for the basis functions, charge density, and potential was used within muffin-tin spheres as well as in the interstitial region. The crystalline space was partitioned into atom-centred polyhedral cell envelopes, and linear muffin-tin orbitals were expanded in spherical harmonics inside the spheres surrounding them. These one-centre expansions define correctly the charge density and the relevant quantities within polyhedra. The cut-off angular momentum in the sums was chosen to maintain the necessary precision. Twelve energy parameters [18] were used to calculate the radial functions for the expansions of the basis in the muffin-tin spheres. Four tail parameters [18] were used to define the kinetic energy of the basis in the interstitial. The values of the parameters were computed automatically by a special algorithm, which took into account change of the crystal energy spectrum under pressure. As a rule, the radii of the muffin-tin spheres were chosen as large as possible, but calculation of each strain was carried out with constant MT radius for all values of the lattice distortion. Integration over the Brillouin zone was done using the linear tetrahedron method. We used 256, 256, and 484 points in the irreducible wedge of the fcc, bcc, and hcp Brillouin zone, respectively. When a strain is introduced in the crystal, the number of points in the irreducible wedge is recalculated for the symmetry of the distorted crystal.

As special analysis showed, the above set-up for calculations made it possible to find for any density the static zero-temperature energy of all structures considered with an accuracy within the limits of 10^{-4} Ryd/atom.

Pressure as a function of volume for $T = 0$ was calculated by differentiation of an analytical expression which approximated the energy–volume relation in the vicinity of each volume value. We considered four frequently used forms of analytical volume dependence of energy [43–47] and chose the Parsafar and Mason [47] formula.

3.2. Free energy and the Gibbs potential

To find the thermodynamic functions at $T > 0$, we used expansion in terms of powers of T to take into account the thermal electronic excitations and a variant of Debye model proposed in [19] to describe thermal excitation of the nuclei.

The contribution of the thermal electronic excitations to the Helmholtz free energy per atom, accurate up to terms of the order of T^2, is connected with the density of states on the Fermi surface $n_F(V)$:

$$F_e(V, T) = -\frac{\pi^2}{6} n_F(V) T^2. \tag{34}$$

The function $n_F(V)$ is calculated in the course of the electronic structure calculation.

The main idea [19] is to derive the dependence of the Debye temperature Θ on the volume by determining how the mean velocity of sound depends on the volume. The Debye temperature and the mean velocity of sound are related as follows:

$$\Theta(V) = \left(\frac{6\pi^2}{V}\right)^{1/3} \hbar \overline{u}(V), \tag{35}$$

where $\overline{u}$ is the mean velocity of sound which can be determined for each value of the volume per atom V by averaging the true velocity of sound $u_s(\vec{n})$ over the directions of the unit vector

$\vec{n}$ and spectrum branches $s = 1, 2, 3$ using the formula [48]

$$\frac{1}{\overline{u}^3} = \frac{1}{3}\sum_s \int \frac{\mathrm{d}\vec{\Omega}}{4\pi}\frac{1}{u_s^3(\vec{n})}. \tag{36}$$

According to [37], if the initial isotropic pressure P affects an anisotropic crystal, then the sound velocity $u_s(\vec{n})$ in direction $\vec{n}$ can be found from the eigenvalue problem for the matrix $L_{ik}(\vec{n})$ completely determined by the elastic constants and initial pressure:

$$L_{ik}(\vec{n}) = \sum_{jl} C_{ijkl} n_j n_l - P\delta_{ik}. \tag{37}$$

The equation has the form

$$\det[L_{ik}(\vec{n}) - \rho u^2(\vec{n})\delta_{ik}] = 0, \tag{38}$$

where ρ is the crystal density. Having theoretically calculated the dependence of the elastic constants on the volume for various structures, we can use formulae (35)–(38) to determine how the Debye temperature depends on volume and calculate the phonon contribution to the Helmholtz free energy per atom:

$$F_i(V,T) = \frac{9}{8}\Theta + 9T\left(\frac{T}{\Theta}\right)^3 \int_0^{\Theta/T} x^2 \ln(1 - \mathrm{e}^{-x})\,\mathrm{d}x. \tag{39}$$

The Helmholtz free energy per atom $F(V,T)$ and Gibbs potential per atom $G(P,T)$ for each crystalline structure are calculated using well-known formulae:

$$F(V,T) = E_c(V) + F_i(V,T) + F_e(V,T), \tag{40}$$

$$G(P,T) = F(V(P,T),T) + PV(P,T). \tag{41}$$

Here $E_c(V)$ is the static zero-temperature energy.

4. Calculation results

4.1. Equation of state and elastic constants

Table 1 lists the calculated specific volume V_0, the bulk modulus B_0 and its pressure derivative B_0', and elastic constants C_{11}, C_{12}, C_{44} for aluminium at zero pressure. Corresponding experimental data for V_0 [49], B_0 [49], B_0' [49], C_{11}, C_{12}, and C_{44} [50] and extrapolations of these data to $T = 0$ are also listed in table 1. We do not cite the corresponding values calculated by other authors and listed, for example, in [6]. In our opinion, it is difficult to reach general conclusions on the basis of results obtained at different times by different numerical methods, using different forms of exchange–correlation functional, and having different and often unknown accuracies.

Total energies of the static lattice and corresponding pressures were calculated for fcc, bcc, and hcp aluminium at 16 values of the specific volume, $V/\tilde{V}_0$, ranging from 1.1 to 0.3. Here $\tilde{V}_0$ is the measured specific volume at atmospheric pressure and temperature 298 K, equal to 112.04 au/atom of the crystal [49]. The equilibrium values of the ratio c/a for each specific volume of the hcp structure were found from the condition of minimum total energy as a function of c/a. Calculated regardless of the impact of zero-point vibrations, the Gibbs potentials at $T = 0$, relative to fcc structure, for bcc and hcp structures are shown in figure 1(a).

To calculate the elastic constants of the bcc and fcc structures, to test relationship (26), and to assess the precision of the elastic constant calculation, we applied five independent strains to each of these structures. The parametrizations that we used for these strains are given in table 2. Strains 1–3 are not volume-conserving and strains 4–5 are strictly volume-conserving.

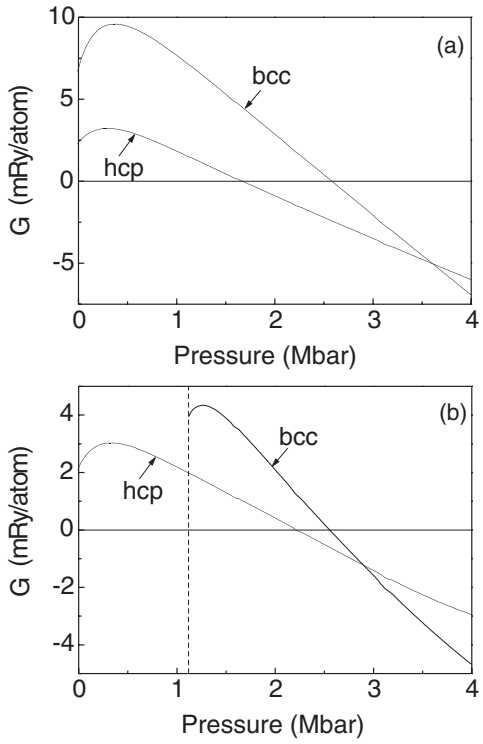

Figure 1. Gibbs potential difference $\Delta G = G - G_{\mathrm{fcc}}$ at $T = 0$ versus pressure for bcc and hcp structures of Al: (a) disregarding and (b) considering the impact of zero-point vibrations.

Table 1. Values of some parameters of fcc aluminium at $T = 298$ and 0 K.

	Experiment, $T = 298$ K	Extrapolation to $T = 0$ K	Calculation without zero-point vibrations	Calculation with zero-point vibrations
V_0 (au)	112.04[a]	110.61	112.22	113.50
B_0 (Mbar)	0.727[a]	0.758	0.744	0.725
B_0'	4.30 [a]	3.97	4.64	4.15
C_{11} (Mbar)	1.069[b]	1.143	1.105	—
C_{12} (Mbar)	0.608[b]	0.619	0.580	—
C_{44} (Mbar)	0.282[b]	0.316	0.311	—

[a] Reference [49].
[b] Reference [50].

We calculated the total energy of each strain for a number of small values of γ. These energies were then fitted to a polynomial in γ and the curvature of the energy versus γ curve was obtained for use in equation (13).

We used strains 1–3 to obtain the elastic constants from systems of equations like (13). The results are presented in table 3. They illustrate the compression dependence of the elastic constants at $T = 0$ for bcc and fcc aluminium.

As mentioned above, the equality $\tilde{C}_{11} - |\tilde{C}_{12}| = 0$ is a condition of violation of the mechanical stability of cubic crystal. It follows from table 3 that the bcc structure is stable

Table 2. The strains used to calculate the elastic constants of the bcc and fcc Al. The energy second derivatives were obtained from equation (13).

Strain	Parameters (unlisted: $\varepsilon_{ij} = 0$)	$\rho_1 \dfrac{\partial^2 E(\rho_1, \gamma)}{\partial \gamma^2}\Big\vert_{\gamma=0}$
1	$\varepsilon_{11} = \varepsilon_{22} = \gamma$	$2(C_{11} + C_{12} - P)$
2	$\varepsilon_{13} = \varepsilon_{31} = \gamma$	$4C_{44} - 2P$
3	$\varepsilon_{11} = \gamma$	$C_{11} - P$
4	$\varepsilon_{11} = \varepsilon_{22} = \gamma$, $\varepsilon_{33} = (1+\gamma)^{-2} - 1$	$6(C_{11} - C_{12}) - 12P$
5	$\varepsilon_{12} = \varepsilon_{21} = \gamma$, $\varepsilon_{33} = (1-\gamma^2)^{-1} - 1$	$4(C_{44} - P)$

Table 3. Second-order elastic constants with addition of the pressure from equation (31) (in Mbar) versus relative volume for fcc and bcc aluminium.

$V/\tilde{V}_0$	$\tilde{C}'_{\rm fcc}$	$\tilde{C}'_{\rm bcc}$	$\tilde{C}^{\rm fcc}_{44}$	$\tilde{C}^{\rm bcc}_{44}$
1.000	0.2529	−0.1720	0.3119	0.4445
0.900	0.3962	−0.1954	0.5557	0.7196
0.800	0.6980	−0.1952	0.9905	1.145
0.700	0.9187	−0.1259	1.662	1.886
0.626	1.017	5.0×10^{-5}	2.350	2.708
0.600	1.039	0.073 86	2.677	3.063
0.500	0.9804	0.5915	4.346	4.828
0.450	0.7427	1.060	5.593	6.053
0.400	0.2105	1.774	7.337	7.595
0.350	−0.8966	2.935	9.832	9.593
0.300	−3.148	5.292	13.11	12.16

only at relative volumes $V/\tilde{V}_0 < 0.626$; the fcc structure becomes mechanically unstable at relative volumes $V/\tilde{V}_0 < 0.4$.

The bulk modulus calculated from equation (20) was used to assess the precision of the elastic constant calculation. We calculated the bcc and fcc elastic constants of Al, using the strains 4–5 and relationship (26). The difference between the elastic constants calculated in this way and the ones obtained using strains 1–3 is within 3% over the whole range of pressures under study.

We applied the five strains listed in table 4 in order to determine the elastic constants of hcp structure Al. All these strains are volume-non-conserving. The atomic positions were optimized at all strains where they had some degrees of freedom. The compression dependences of the elastic constants at $T = 0$ for hcp aluminium are presented in table 5. Figure 2 shows mean sound velocity $\overline{u}$ versus compression calculated using equation (36) for the three aluminium structures. The non-monotonic variation of the curves in figure 2 with the growth of pressure is an interesting peculiarity. The mean sound velocities differ significantly in the three aluminium structures considered, which allows reliable detection of structural changes on the basis of the sound velocity measurements.

4.2. Debye temperature and Grüneisen parameter

Using the calculated values of the elastic constants and formulae (35)–(38), we calculated the volume dependence of the Debye temperature for the above aluminium structures. The data

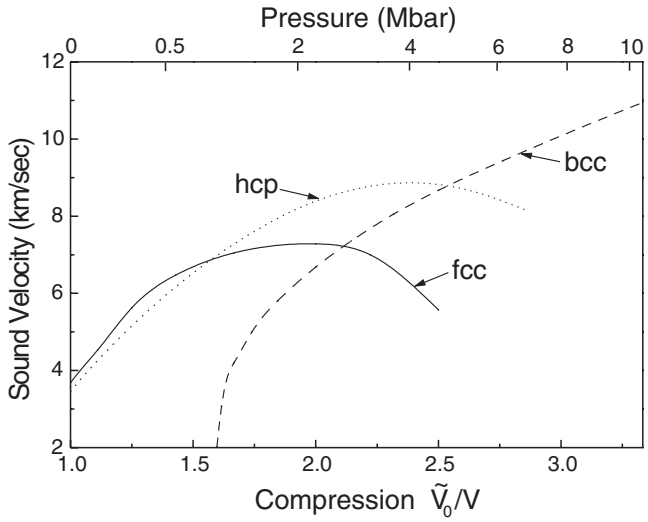

Figure 2. Mean sound velocity for fcc, bcc, and hcp aluminium. Pressures marked on the upper axis correspond to compressions of the fcc structure on the lower axis.

Table 4. The strains used to calculate the elastic constants of hcp Al. The energy second derivatives were obtained from equation (13).

Strain	Parameters (unlisted: $\varepsilon_{ij} = 0$)	$\rho_1 \dfrac{\partial^2 E(\rho_1, \gamma)}{\partial \gamma^2}\Big\vert_{\gamma=0}$
1	$\varepsilon_{11} = \varepsilon_{33} = \gamma$	$C_{11} + 2C_{13} + C_{33} - 2P$
2	$\varepsilon_{11} = -\varepsilon_{22} = \gamma$	$2(C_{11} - C_{12} - P)$
3	$\varepsilon_{11} = \varepsilon_{22} = \gamma$	$2(C_{11} + C_{12} - P)$
4	$\varepsilon_{13} = \varepsilon_{31} = \gamma$	$4C_{44} - 2P$
5	$\varepsilon_{33} = \gamma$	$C_{33} - P$

Table 5. Second-order elastic constants with addition of pressure from equation (31) (in Mbar) versus relative volume for hcp aluminium.

$V/\tilde{V}_0$	$\tilde{C}_{11}^{\mathrm{hcp}}$	$\tilde{C}_{12}^{\mathrm{hcp}}$	$\tilde{C}_{13}^{\mathrm{hcp}}$	$\tilde{C}_{33}^{\mathrm{hcp}}$	$\tilde{C}_{44}^{\mathrm{hcp}}$
1.00	1.394	0.4138	0.4978	1.355	0.1402
0.70	5.116	1.854	1.710	5.285	0.8427
0.50	13.02	5.353	4.623	13.65	2.405
0.40	20.42	12.99	8.504	23.50	3.990
0.35	25.48	20.76	12.36	31.85	5.048
0.30	31.73	33.04	18.88	44.60	6.207

obtained are presented in table 6. Differentiating the dependence of the Debye temperature on volume readily gives the dependence of the Grüneisen parameter on volume:

$$\gamma(V) = -\frac{\mathrm{d} \ln \Theta(V)}{\mathrm{d} \ln V}. \tag{42}$$

Figure 3 shows our data and the Grüneisen parameter calculated from the Slater formula [51]

$$\gamma_{Slat}(V) = -\frac{2}{3} - \frac{V}{2}\frac{\mathrm{d}^2 P_{col}}{\mathrm{d}V^2}\left(\frac{\mathrm{d}P_{col}}{\mathrm{d}V}\right)^{-1}, \tag{43}$$

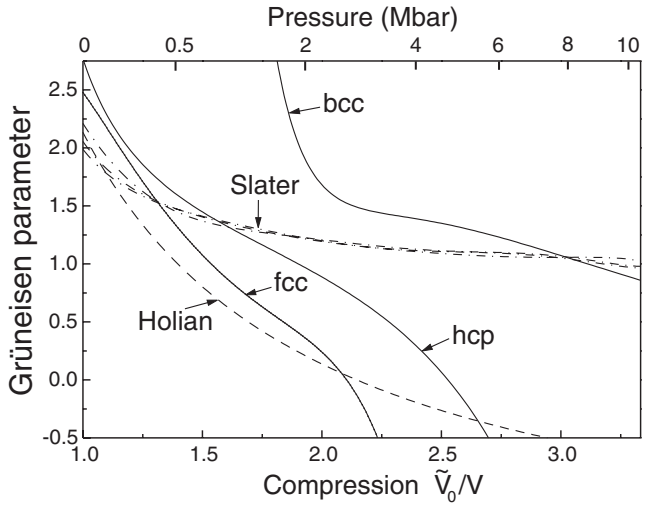

Figure 3. The Grüneisen parameters for fcc, bcc, and hcp aluminium. The solid curve shows our calculations, the dashed one shows data from the semi-empirical EOS [52] for fcc structure, and the dot–dash curve shows the calculation with the Slater formula. Pressures marked on the upper axis correspond to compressions of the fcc structure on the lower axis.

for the three aluminium structures. Here P_{col} is the pressure at $T = 0$ K. The figure also shows the dependence described by the formula

$$\gamma(V) = 2.136 + 4\left[\frac{V}{\tilde{V}_0} - 1\right], \tag{44}$$

that is used for the Grüneisen parameter in the semi-empirical EOS [52]. Our calculations show that in the range of compressions considered, the Grüneisen parameters of fcc, bcc, and hcp aluminium are fundamentally different instead of being almost the same as they would be according to the Slater formula. For the fcc structure our results are close both qualitatively and quantitatively to semi-empirical formula (44), while the values of the Grüneisen parameter obtained using the Slater formula agree with it only for small compressions. This result is a consequence of the fact that our approach is more accurate than the Slater formula in describing how the vibrational free energy of the lattice ions depends on the crystal structure. Our Grüneisen parameter differs from that obtained in terms of the mean-field potential [15] for the same reason.

Using the expression for the energy of zero-point vibrations per atom in the Debye model:

$$E_0(V) = \tfrac{9}{8}k\Theta_D(V), \tag{45}$$

where k is Boltzmann's constant, one can calculate the contribution of zero-point vibrations to pressure, and the bulk modulus and its pressure derivative. The last column of table 1 contains these values obtained taking into account zero-point vibrations of nuclei at zero pressure. Gibbs potentials for bcc and hcp structures relative to fcc structure, calculated considering the impact of zero-point vibrations, are shown in figure 1(b).

Moreover, we calculated the 300 K isotherm and Hugoniot using the Debye temperature and density of states on the Fermi surface as functions of volume in the equation for free energy (40). They are shown in figures 4 and 5, respectively, along with experimental data and data obtained from the semi-empirical EOS. Since our EOS does not contains a single parameter determined from the experimental data and is completely based on the *ab initio*

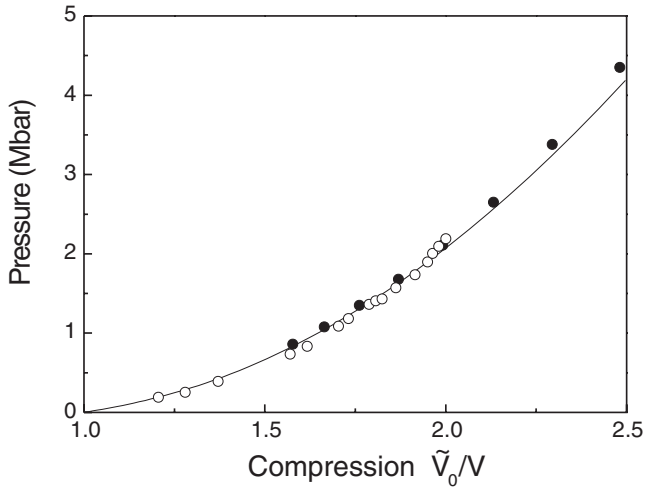

Figure 4. The theoretical 300 K isotherm for aluminium (solid curve), compared with room temperature diamond-anvil-cell measurements [53] (open circles) and a 300 K isotherm deduced from shock data [54] (solid circles).

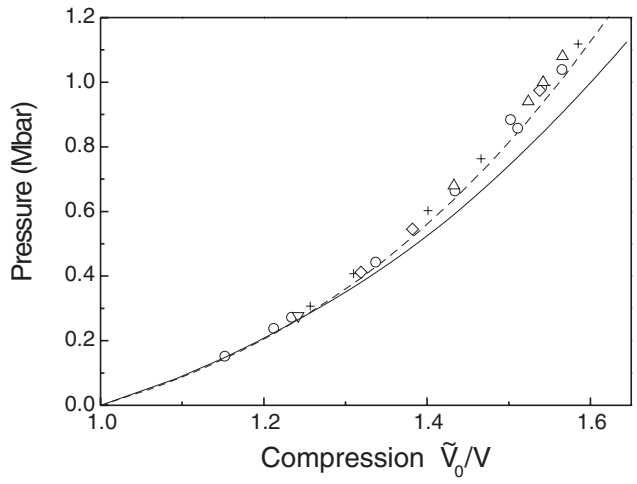

Figure 5. Comparison of the calculated Hugoniot (——) for aluminium with the Hugoniot obtained from the semi-empirical EOS [55] (– – –) and the experimental data of Mitchel and Nellis [56] (+), Al'tshuler *et al* [57] (○), Al'tshuler *et al* [58] (◇), Neal [59] (▽), McQueen *et al* [60] (△).

calculations, the agreement can be considered satisfactory—especially so because our EOS is not intended to replace the semi-empirical EOS; its purpose is to give information in cases when there are no experimental data or direct experiment is not feasible.

4.3. The relative stability diagram for fcc, bcc, and hcp Al

Having thermodynamic functions for $T > 0$, we tried to plot a relative stability diagram for fcc, bcc, and hcp aluminium structures in coordinates (P, T) by comparing the Gibbs thermodynamic potentials of these three structures. Similarly, the relative stability diagram

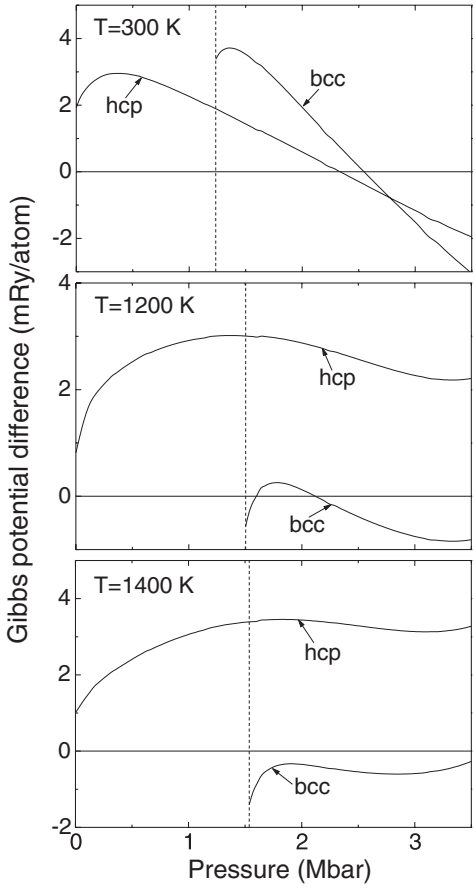

Figure 6. Gibbs potential difference $\Delta G = G - G_{\mathrm{fcc}}$ of bcc and hcp aluminium versus pressure for three isotherms: $T = 300$, 1200, and 1400 K. The pressure axis includes the thermal pressure.

Table 6. Debye temperature versus relative volume for fcc, bcc, and hcp aluminium.

$V/\tilde{V}_0$	Θ_D^{fcc} (K)	Θ_D^{bcc} (K)	Θ_D^{hcp} (K)
1.000	427.89	—	415.44
0.900	546.04	—	—
0.800	704.61	—	—
0.700	847.35	—	834.08
0.626	941.27	275.31	—
0.600	971.14	578.79	—
0.500	1066.4	978.48	1271.8
0.450	1061.6	1165.8	—
0.400	878.81	1367.9	1427.6
0.350	—	1606.8	1345.0
0.300	—	1900.9	—

was plotted for bcc and fcc potassium [12]. A good agreement between the calculated and the experimental phase diagrams for potassium [12], when energies of neighbour structures are very close to each other ($\Delta E \approx 4 \times 10^{-5}$ Ryd), leads us to expect the analogous results for

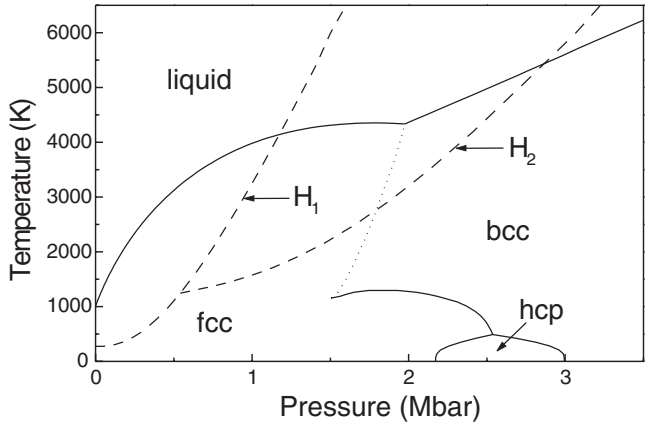

Figure 7. The relative stability diagram for fcc, bcc, and hcp aluminium in coordinates (P, T). The dotted curve is the boundary of the mechanical stability region of bcc structure, dashed curves show the single-stage compression Hugoniot and one of the two-stage compression Hugoniot curves obtained with the semi-empirical EOS [55]. The pressure axis includes the thermal pressure.

aluminium, for which experimental data on phase boundaries are absent, to also be sufficiently accurate. However, for aluminium the problem appears to be more difficult. Here we have a case where a thermodynamically preferable structure becomes mechanically unstable. The problem is illustrated in figure 6, where the Gibbs thermodynamic potentials of bcc and hcp structures are shown relatively to the fcc one at three temperatures.

In figure 7 we show the relative stability diagram in coordinates (P, T) for fcc, bcc, and hcp Al. The phase boundaries, that were found by comparing the Gibbs thermodynamic potentials of the fcc, bcc, and hcp aluminium structures, are shown in figure 7 as solid curves. The melting curve was obtained using the Lindeman criterion

$$T_m = \text{constant} \times V^{2/3}\Theta_D^2(V) \tag{46}$$

and the experimental melting point at atmospheric pressure. It is shown as a solid curve, too. Dashed curves are a single-stage compression Hugoniot and the two-stage compression Hugoniot obtained from the semi-empirical EOS [55]. The boundary of mechanical stability for bcc aluminium is marked with dots. It is described by the equation

$$V_{\text{bcc}}(P, T) = V_b, \tag{47}$$

where V_b is the specific volume for which $\tilde{C}_{11}$ is equal to $|\tilde{C}_{12}|$. According to our calculations, bcc structure has the lowest thermodynamic potential near this boundary at temperatures above $\sim$1000 K. Hence, a direct fcc–bcc transition is impossible at temperatures above $\sim$1000 K. Therefore, a structure different from those considered must exist at such temperatures, and the fcc structure transforms into it to ensure the continuity of the thermodynamic potential. This Al structure change into bcc structure upon further compression. We are now exploring what structure is intermediate between fcc and bcc.

5. Conclusions

We performed a set of first-principles, self-consistent, total-energy calculations with the FPLMTO method to determine the EOS and the elastic constants of the fcc, bcc, and hcp Al structures at $T = 0$. The specific volume, bulk moduli, and elastic constants that we calculated

for the fcc structure at zero pressure are in a good agreement with available experimental data. We used elastic constants to calculate the contribution of the thermal excitation of the nuclei to thermodynamic functions and to predict the form of the relative stability diagram of the fcc, bcc, and hcp Al structures on the basis of the Debye model. Our calculations show that at pressures within 1–2 Mbar and temperatures $T > 1000$ K, the aluminium structure must have a lower symmetry compared with the structures considered. It would be very interesting to verify this outcome experimentally. It is not improbable that the same effect as was described by Neaton and Ashcroft [61] occurs in aluminium at $T > 0$.

Acknowledgments

The authors are grateful to D Yu Savrasov and S Yu Savrasov for providing their version of a code realizing the method described in [18]. They also thank D Yu Savrasov and E G Maximov for very helpful discussions of the details of the method [18]. This work was supported by the Russian Foundation for Basic Research (grants Nos 01-02-18044 and 01-02-16108).

References

[1] McMahan A K and Moriarty J A 1983 *Phys. Rev.* B **27** 3235
[2] Lam P K and Cohen M L 1983 *Phys. Rev.* B **27** 5986
[3] Boettger J C and Trickey S B 1984 *Phys. Rev.* B **29** 6434
[4] Rodríguez C O, Cappannini O M, Peltzer y Blancá E L and Casali R A 1987 *Phys. Status Solidi* b **142** 353
[5] Boettger J C and Trickey S B 1995 *Phys. Rev.* B **51** 15 623
[6] Boettger J C and Trickey S B 1996 *Phys. Rev.* B **53** 3007
[7] Sin'ko G V and Smirnov N A 1999 *Phys. Met. Metallogr.* **87** 370
[8] Zel'dovich Ya B and Raizer Yu P 1967 *Physics of Shock Waves and High-Temperature Hydrodynamic Phenomena* vols 1 and 2 (New York: Academic)
[9] Moruzzi V L, Janak J F and Schwarz K 1988 *Phys. Rev.* B **37** 790
[10] Sin'ko G V and Smirnov N A 1999 *Phys. Met. Metallogr.* **87** 374
[11] Christensen N E, Boers D J, van Velsen J L and Novikov D L 2000 *J. Phys.: Condens. Matter* **12** 3293
[12] Katsnelson M I, Sin'ko G V, Smirnov N A, Trefilov A V and Khromov K Yu 2000 *Phys. Rev.* B **61** 14 420
[13] Debernardi A, Alouani M and Dreyssé H 2001 *Phys. Rev.* B **63** 064305
[14] Mohn P, Schwarz K and Blaha P 1996 *J. Phys.: Condens. Matter* **8** 817
[15] Wang Y and Li L 2000 *Phys. Rev.* B **62** 196
[16] Strachan A, Çağin T and Goddard W A III 1999 *Phys. Rev.* B **60** 15 084
[17] Cohen R E and Gülseren O 2001 *Phys. Rev.* B **63** 224101
[18] Savrasov S Yu and Savrasov D Yu 1992 *Phys. Rev.* B **46** 12 181
[19] Sin'ko G V and Kutepov A L 1996 *Phys. Met. Metallogr.* **82** 129
[20] Sin'ko G V and Smirnov N A 2000 *Proc. 15th Int. Conf. on Equations of State for Matter (Terskol)* (Chernogolovka: Institution of Chemical Physics Problems) p 20
[21] Sin'ko G V and Smirnov N A 2000 *Proc. Russia Conf. on Phase Transitions under High Pressure (Chernogolovka)* (Chernogolovka: Institution of Chemical Physics Problem) p U/16
[22] Sin'ko G V and Smirnov N A 2000 *Proc. Int. Conf. on Shock Waves in Condensed Matter (Saint Petersburg)* (St Petersburg: High Pressure Centre) p 126
[23] Mehl M J, Osburn J E, Papaconstantopoulos D A and Klein B M 1990 *Phys. Rev.* B **41** 10 311
[24] Osburn J E, Mehl M J and Klein B M 1991 *Phys. Rev.* B **43** 1805
[25] Alouani M, Albers R C and Methfessel M 1991 *Phys. Rev.* B **43** 6500
[26] Söderlind P, Eriksson O, Wills J M and Boring A M 1993 *Phys. Rev.* B **48** 5844
[27] Söderlind P, Eriksson O, Wills J M and Boring A M 1993 *Phys. Rev.* B **48** 9306
[28] Fast L, Wills J M, Johansson B and Eriksson O 1995 *Phys. Rev.* B **51** 17 431
[29] Mehl M J and Papaconstantopoulos D A 1996 *Phys. Rev.* B **54** 4519
[30] Tse J S, Klug D D, Uehara K, Li Z Q, Haines J and Léger J M 2000 *Phys. Rev.* B **61** 10 029
[31] Guo G Y and Wang H H 1995 *Phys. Rev.* B **62** 5136
[32] Beckstein O, Klepeis J E, Hart G L W and Pankratov O 2001 *Phys. Rev.* B **63** 134112
[33] Jansen H J F and Freeman A J 1987 *Phys. Rev.* B **35** 8207

[34] Iitaka T and Ebisuzaki T 2001 *Phys. Rev.* B **65** 012103
[35] Jochym P T and Parlinski K 2001 *Phys. Rev.* B **65** 024106
[36] Gülseren O and Cohen R E 2001 *Phys. Rev.* B **65** 064103
[37] Wallace D C 1970 *Solid State Physics* vol 25 (New York: Academic) p 301
[38] Kittel C 1996 *Introduction to Solid State Physics* (New York: Wiley)
[39] Vaks V G, Zarochentsev E V, Kravchuk S P and Safronov V P 1978 *J. Phys. F: Met. Phys.* **8** 725
[40] Wang J, Li J, Yip S, Phillpot S and Wolf D 1995 *Phys. Rev.* B **52** 12 627
[41] Perdew J P and Wang Y 1992 *Phys. Rev.* B **45** 13 244
[42] Perdew J P, Chevary J A, Vosko S H, Jackson K A, Pederson M R, Singh D J and Fiolhais C 1992 *Phys. Rev.* B **46** 6671
[43] Murnaghan F D 1944 *Proc. Natl Acad. Sci. USA* **30** 244
[44] Birch F 1978 *J. Geophys. Res.* **83** 1257
[45] Rose J H, Smith J R, Guinea F and Ferrante J 1984 *Phys. Rev.* B **29** 2963
[46] Dodson B W 1987 *Phys. Rev.* B **35** 2619
[47] Parsafar G and Mason E A 1994 *Phys. Rev.* B **49** 3049
[48] Ashcroft N W and Mermin N D 1976 *Solid State Physics* (Ithaca, NY: Cornell University Press)
[49] Syassen K and Holzapfel W B 1978 *J. Appl. Phys.* **49** 4427
[50] Kamm G N and Alers G A 1964 *J. Appl. Phys.* **35** 327
[51] Slater J C 1939 *Introduction to Chemical Physics* (New York: McGraw-Hill)
[52] Holian K S 1986 *J. Appl. Phys.* **59** 149
[53] Greene R G, Luo H and Ruoff A L 1994 *Phys. Rev. Lett.* **73** 2075
[54] Nellis W J, Moriarty J A, Mitchell A C, Ross M, Dandrea R G, Ashcroft N W, Holmes N C and Gathers G R 1988 *Phys. Rev. Lett.* **60** 1414
[55] Sapozhnikov A T and Pershina A V 1979 *VANT: Numerical Methods and Codes for Problems in Computational Physics* vol 4 (Moscow: Central Institution of Information and Technical–Economic Investigations for Atomic Science and Technics) p 47
[56] Mitchel A C and Nellis W J 1981 *J. Appl. Phys.* **52** 3363
[57] Al'tshuler L V, Bakanova A A, Dudoladov I P, Dynin E A, Trunin R F and Chekin B S 1981 *Sov. J. Appl. Mech. Tech. Phys.* **22** 145
[58] Al'tshuler L V, Kormer S B, Brazhnik M I, Vladimirov L A, Speranskaya M P and Funtikov A I 1960 *Zh. Eksp. Teor. Fiz.* **38** 1061
[59] Neal T 1975 *J. Appl. Phys.* **46** 2521
[60] McQueen R G, Fritz J M and Morris C E 1984 *Shock Waves in Condensed Matter* vol 83, ed J R Asay, R A Graham and G K Straub (Amsterdam: North-Holland) p 95
[61] Neaton J B and Ashcroft N W 1999 *Nature* **400** 141